

Energy transfer from baryons to dark matter as a unified solution to small-scale structure issues of the Λ CDM model

A. Del Popolo,^{1,2,3} Francesco Pace,⁴ Morgan Le Delliou,^{5,6} and Xiguo Lee⁷

¹*Dipartimento di Fisica e Astronomia, University Of Catania, Viale Andrea Doria 6, 95125, Catania, Italy*

²*Institute of Modern Physics, Chinese Academy of Sciences,
Post Office Box 31, Lanzhou 730000, Peoples Republic of China*

³*INFN sezione di Catania, Via S. Sofia 64, I-95123 Catania, Italy **

⁴*Jodrell Bank Centre for Astrophysics, School of Physics and Astronomy,
The University of Manchester, Manchester, M13 9PL, United Kingdom †*

⁵*Institute of Theoretical Physics, Physics Department, Lanzhou University, No.222,
South Tianshui Road, Lanzhou, Gansu, 730000, Peoples Republic of China*

⁶*Instituto de Astrofísica e Ciências do Espaço, Universidade de Lisboa,
Faculdade de Ciências, Ed. C8, Campo Grande, 1769-016 Lisboa, Portugal ‡*

⁷*Institute of Modern Physics, Chinese Academy of Sciences,
Post Office Box 31, Lanzhou, Gansu 730000, Peoples Republic of China §*

(Dated: March 10, 2024)

Using a semianalytic code, we show how baryon physics in a Λ CDM cosmology could solve the discrepancy between numerical predictions of dark matter haloes and observations, ranging from dwarf galaxies to clusters, without the need of nonstandard dark matter models as advocated, for example, by [Kaplighat *et al.*, *Phys. Rev. Lett.* **116**, 041302, (2016)]. Combining well established results, we show, for the first time, how accounting for baryon physics, in particular dynamical friction mechanisms, leads to flat galaxy-cluster profiles and correlations in several of their properties, solves the so-called “diversity problem” and reproduces very well the challenging, extremely low-rising rotation curve of IC2574. We therefore suggest treating baryonic physics properly before introducing new exotic features, albeit legitimate, in the standard cosmological model.

I. INTRODUCTION

The Λ CDM model, while very successful [1, 2], presents some issues (e.g., [3, 4]). Particularly troublesome is the discrepancy between the flat density profiles of dark-matter (DM)-dominated dwarf galaxies, irregulars and low surface brightness galaxies (hereafter LSBs), high surface brightness spiral galaxies, in some cluster of galaxies, and the cuspy profile predicted by dissipationless N-body simulations (e.g., [5]), dubbed cusp/core problem [6–8]. Better understood in terms of the excess of DM in the inner parts of the galaxies rather than of the inner slope, it connects to the too-big-to-fail (TBTf) problem [9, 10]. We also mention the large diversity (hereafter dubbed “diversity problem” in analogy to other works) in the dwarf-galaxies rotation curves (RCs), which are at odds with hydrodynamic simulations¹.

A possible solution to these problems is to assume that the DM component is not cold and this leads to a wealth of different models (e.g., self-interacting DM (SIDM) models [11]) recently used by [12] to propose a unified solution (at all scales) to the small scale problems of the Λ CDM model.

The study of [12] claims the difficulty or impossibility for the Λ CDM model to explain the rotation curve of IC2574 and several other issues, and, in an attempt to solve them, proposes the SIDM model as a possible alternative to the Λ CDM model.

It is thus of fundamental importance to verify whether the Λ CDM model can solve, at all scales, the problems discussed in [12].

In the present paper we want to address the following question: does a unified solution exist to the “deficit problem in halos” in the Λ CDM model without invoking a different physics? We will closely follow [12] in showing how the “deficit problem in halos” is solved when baryonic physics is taken into account in the Λ CDM model.

The plan of this work is as follows: we first present our semianalytical model in Sec. II. Differently from N-body and hydrodynamical simulations, the model presents the various physical contributions more clearly and allows to disentangle them more easily. We then show, in Sec. III, how it reproduces the clusters (e.g., A2537) presented in [13, 14], how it explains the RCs of some peculiar galaxies (e.g., IC 2574, this one fitted by [15] using SIDM and baryon physics) in Sec. IV, and how it solves the diversity problem discussed by [16] in Sec. V. Finally we conclude in Sec. VI discussing our results in comparison to those of [12].

II. MODEL

Here we recall the model used above. First introduced by [17, 18], many of its features were developed in [19–21], and allowed studies of the density profiles’ universality [22, 23], of the density profile of galaxies [24–26] and clusters [25, 27], and of the inner surface-density of galaxies [28].

The model is a strong improvement of the original spherical collapse model [29–34], and includes the effects of random angular momentum due to random motions arising in the col-

* Corresponding author. adelpopolo@oact.inaf.it

† francesco.pace@manchester.ac.uk

‡ delliou@ift.unesp.br

§ xgl@impcas.ac.cn

¹ Note that the Λ CDM model suffers from others drawbacks like the cosmological constant problem [3, 4], and the cosmic coincidence problem.

lapse phase (e.g., [32, 34]) and ordered angular momentum (e.g., [35–37]) from tidal torques, dark energy [38–41], dynamical friction arising from the interaction between baryons and DM [17, 42–49], adiabatic contraction (e.g., [50–53]), gas cooling, star formation, photoionization, supernovae and AGN feedback [54–56].

At this stage we want to stress that the main mechanism of the model resides in the dynamical friction and as described in point 5 (see the following), the other mechanisms (e.g. SN feedback) are only contributing at the percent level.

The main evolutionary phases present in the model are listed as follows:

1. In the linear phase the DM and the diffuse gas proto-structure expand to a maximum radius, then DM re-collapses, forming the potential well for baryons to fall into.
2. Baryons are subject to radiative processes and form stars, condense forming clumps which collapse in the centre of the halo.
3. While baryons are compressed during the collapse phase and make the DM profile more cuspy, the formed clumps interact with the DM component and stars via dynamical friction (DF) and transfer energy and angular momentum (AM) [57–59] with the result of having DM particles moving away from the centre leading to a net reduction of the central density [42, 43]. This process leads to the formation of cores in dwarf spheroidals and spirals, while giant galaxies keep a steeper profile due to their deeper potential wells.
4. The effect of DF is amplified by tidal torques and random AM.
5. Finally, in a later phase, supernovae explosions expel gas lowering the stellar density and disrupting smallest gas clumps after their partial conversion into stars (see [49]). The expulsion of gas has the additional effect of enlarging the core (this is quantified in a few percent effect).

II.1. Density profile

The spherical density perturbation model follows the perturbation evolution from the expansion due to the Hubble flow till the turn-around and then into collapse [60, 61]. The final profile of the perturbation is given by

$$\rho(x) = \frac{\rho_{\text{ta}}(x_m)}{f(x_i)^3} \left[1 + \frac{d \ln f(x_i)}{d \ln g(x_i)} \right]^{-1}, \quad (1)$$

where x_i is the initial radius, $f(x_i) = x/x_m(x_i)$ the collapse factor, $\rho_{\text{ta}}(x_m)$ the turn-around density and $x_m(x_i)$ the turn-around radius, which can be written as

$$x_m = g(x_i) = x_i \frac{1 + \bar{\delta}_i}{\bar{\delta}_i - (\Omega_i^{-1} - 1)}. \quad (2)$$

In the above expression, Ω_i represents the matter density parameter and $\bar{\delta}_i$ the average overdensity inside a shell of DM and baryons. Initially, in the gas phase, the “universal baryon fraction” is set to $f_b = 0.17 \pm 0.01$ (0.167 in [2, 62]) and evolves, due to star formation processes, as follows.

Using the tidal torque theory (TTT), one can evaluate the “ordered angular momentum” h induced by tidal torques exerted by large scale structures on smaller scales [35, 63–67]. At the same time, the “random angular momentum” j depends on the eccentricity $e = r_{\text{min}}/r_{\text{max}}$ [68], being r_{max} the apocentric radius, and r_{min} the pericentric radius. One needs to correct the eccentricity for the effects of the dynamical state of the system found by [33]:

$$e(r_{\text{max}}) \simeq 0.8 \left(\frac{r_{\text{max}}}{r_{\text{ta}}} \right)^{0.1}, \quad (3)$$

for $r_{\text{max}} < 0.1r_{\text{ta}}$, being $r_{\text{ta}} = x_m(x_i)$ the spherically averaged turn-around radius.

The steepening of the profile due to adiabatic compression is calculated iteratively [69] and follows the prescription of [51], while dynamical friction is modelled by a force in the equation of motions (see [17], Eq. (A14)).

II.2. Baryons, discs, and clumps

Baryons are initially modelled in a gas phase and settle into a rotationally supported stable disk for spiral galaxies. The disc sizes and masses obtained from the model have been shown to solve the angular momentum catastrophe (AMC) (Sect. 3.2, Figs. 3, and 4 of [25]), producing discs with sizes and masses similar to those of real galaxies.

However, denser discs are unstable, as known from the Jeans’ criterion, despite the shear force stabilisation. Toomre [70] gave the disc instability and clump formation condition

$$Q \simeq \frac{\sigma \Omega}{\pi G \Sigma} = \frac{c_s \kappa}{\pi G \Sigma} < 1, \quad (4)$$

with σ the 1-D velocity dispersion,² Ω the angular velocity, Σ the surface density, c_s the adiabatic sound speed, and κ the epicyclic frequency. The fastest growing mode derives from the perturbation dispersion relation when $Q < 1$, and is the solution of $d\omega^2/dk = 0$, giving $k_{\text{inst}} = \frac{\pi G \Sigma}{c_s^2}$ (see [49, 71]). We used that condition to obtain the clumps radii for our galaxy [72]

$$R \simeq 7G\Sigma/\Omega^2 \simeq 1\text{ kpc}. \quad (5)$$

Marginally unstable discs ($Q \simeq 1$) with maximal velocity dispersion have a total mass three times larger than that of the cold disc, form clumps with mass $\simeq 10\% M_d$ [73], where M_d is the mass of the disk.

² In most galaxies hosting clumps $\sigma \simeq 20 - 80$ km/s.

Objects of masses few times $10^{10} M_{\odot}$, and found in $5 \times 10^{11} M_{\odot}$ haloes at $z \simeq 2$, stay in a marginally unstable phase for $\simeq 1$ Gyr. In general we found that the main properties of clumps are similar to those found by [74].

In agreement with [17, 44–49, 75, 76], energy and AM transfer from clumps to DM flatten the profile more efficiently in smaller haloes.

II.2.1. Clumps lifetime

The clumps discussed above have been observed both in simulations (e.g., [77–83]) and observations.

Clumpy structures, dubbed chain galaxies, and clump clusters are observed in high-redshift galaxies [84–86], while massive star-forming clumps [87, 88] were found in HST Ultra Deep Field observations, in a large number of star-forming $z = 1 - 3$ galaxies [89], and even in deeper fields up to $z \simeq 6$ [90].

Very gas-rich disc experiencing radiative cooling in the dense accreting gas induces self-gravity instability that should form those clumpy structures (e.g., [74, 77, 91–93]).

The clump’s lifetime is crucial in the processes described above: they should transform the cusp into a core, before disruption by stellar feedback, by sinking to the galaxy centre. The mass fraction lost by stellar feedback, e , and that transformed into stars $\epsilon = 1 - e$, assess the capacity of the clump to form a bound stellar system. According to simulations and analytic models [94], for $\epsilon \geq 0.5$, most of the stellar mass will remain bound. Estimation by [72] of the expulsion fraction $e = 1 - \epsilon = 0.86(\Sigma_1 M_9)^{-1/4} \epsilon_{\text{eff},-2}$, with $\Sigma_1 = \frac{\Sigma}{0.1 \text{ g/cm}^2}$, $M_9 = M/10^9 M_{\odot}$, and $\epsilon_{\text{eff},-2} = \epsilon_{\text{eff}}/0.01$, can be obtained using the dimensionless star-formation rate efficiency $\epsilon_{\text{eff}} = \frac{\dot{M}_*}{M/t_{\text{ff}}}$, i.e. the free-fall t_{ff} to depletion time ratio, with stellar mass M_* . For a broad range of densities, size scales and environments, $\epsilon_{\text{eff}} \simeq 0.01$ [95]. For a typical clump with $M \simeq 10^9 M_{\odot}$, $\Sigma \simeq 0.1 \text{ g/cm}^2$ and $\epsilon_{\text{eff}} \simeq 0.01$ one finds $\epsilon \simeq 0.85$ and $e \simeq 0.15$. Thus clumps mass loss is small before they reach the galactic centre. The previous argument and the relation $e = 1 - \epsilon$ are valid for smaller clumps, which are however more compact and the corresponding galaxies smaller, with the final result that clumps reach the centre before being destroyed.

An alternative assessment of clumps disruption compares its lifetime to its central migration time. Dynamical friction and tidal torques are responsible for a migration time of $\simeq 200$ Myrs for a $10^9 M_{\odot}$ mass clump, [49, 86].

For clumps similar to those discussed above, the Sedov-Taylor solution ([86], Eqs. 8,9) yields an expansion timescale similar to the migration time.

Ceverino *et al.* [77] found that in their hydro-dynamical simulations clumps are in Jeans’ equilibrium and rotationally supported and therefore a long lifetime ($\simeq 2 \times 10^8$ Myr) can be inferred. These findings are in agreement with [72] who found that clumps survive if only few percent of the gas is converted into stars, in agreement with the Kennicutt-Schmidt law. All these results confirm previous simulations by [96].

While [79–81] found long-living clumps reaching the centre when properly taking into account stellar feedback, radiative and non-thermal feedback, [78] obtained long-lived objects for any reasonable amount of feedback.

Strong observational evidence of long-lived clumps derives from the estimation of clump ages through gas expulsion, metal enrichment and expansion time scales (respectively 170-1600 Myrs, $\simeq 200$ Myrs and > 100 Myrs) by [86].

Finally, clump stability is supported by observational similitude in radius and mass between low- and high-redshift clumps [97–99].

II.3. Star formation and feedback

The model treatment of gas cooling, star formation, reionisation and supernovae feedback follows the lines of argument of [54, 55].

Reionisation occurs in the redshift range 11.5-15, changing the baryon fraction as [55]

$$f_{\text{b,halo}}(z, M_{\text{vir}}) = \frac{f_{\text{b}}}{[1 + 0.26 M_{\text{F}}(z)/M_{\text{vir}}]^3}, \quad (6)$$

with M_{vir} the virial mass and M_{F} the “filtering mass” (see [100]), while a cooling flow models the gas cooling (e.g., [55, 101], see Sect. 2.2.2).

Star formation occurs after gas settles in a disk, at a rate given by

$$\psi = 0.03 M_{\text{sf}}/t_{\text{dyn}}, \quad (7)$$

resulting in the gas mass conversion into stars

$$\Delta M_* = \psi \Delta t. \quad (8)$$

Here, we denote with M_{sf} the gas mass above the density threshold $n > 9.3/\text{cm}^3$ (fixed as in [102]), and we use the time-step Δt for a disc dynamical time t_{dyn} (see [54], for more details).

Following [103], supernovae feedback (SNF) injects energy for SN explosions as

$$\Delta E_{\text{SN}} = 0.5 \epsilon_{\text{halo}} \Delta M_* \eta_{\text{SN}} E_{\text{SN}}, \quad (9)$$

modelling, for a Chabrier IMF [104], the number of supernovae per solar mass as $\eta_{\text{SN}} = 8 \times 10^{-3}/M_{\odot}$, the disc gas reheating energy efficiency ϵ_{halo} , and the typical SN explosion energy release as $E_{\text{SN}} = 10^{51}$ erg.

The resulting gas reheating depends on the stars formed

$$\Delta M_{\text{reheat}} = 3.5 \Delta M_* . \quad (10)$$

The thermal energy change caused by the reheated gas

$$\Delta E_{\text{hot}} = 0.5 \Delta M_{\text{reheat}} \eta_{\text{SN}} E_{\text{SN}}, \quad (11)$$

induces, if $\Delta E_{\text{SN}} > \Delta E_{\text{hot}}$, ejection of

$$\Delta M_{\text{eject}} = \frac{\Delta E_{\text{SN}} - \Delta E_{\text{hot}}}{0.5 V_{\text{vir}}^2}, \quad (12)$$

hot gas from the halo, with $V_{\text{vir}}^2 = 2\Delta E_{\text{hot}}/\Delta M_{\text{reheat}}$.

A fundamental difference between the SNF model by [102] and ours resides in our cusp flattening starting before star formation, and its energy source being gravitational.

Stellar and supernovae feedback start to take place only after DF formed the core, disrupting the core gas clouds (similarly to [49]).

AGN quenching becomes significant for masses $M \simeq 6 \times 10^{11} M_{\odot}$ [105]. The prescription of [56, 106] leads to our account for AGN feedback: when stellar density exceeds $2.4 \times 10^6 M_{\odot}/\text{kpc}^3$, gas density reaches 10 times that, and the 3D velocity dispersion exceeds 100 km/s, a Super-Massive-Black-Hole (SMBH) is formed, seeded at $10^5 M_{\odot}$. Hence, a modification of the model by [107], as in [56], yields SMBH mass accretion and AGN feedback.

Our model demonstrated its robustness in several ways:

- The cusp flattening from DM heating by collapsing baryonic clumps predicted for galaxies and clusters is in agreement with following studies [42, 43, 45–49]; [23], in Fig. 4, shows a comparison of our model with the SPH simulations of [108].
- The correct shape of galaxies density profiles [17, 18] was predicted before the SPH simulations by [108, 109], and correct clusters density profiles [27] before [110], although the latter use different dominant mechanisms than the former.
- The inner slope dependence on halo mass ([22], Fig. 2a solid line) was predicted before almost the same result was shown in Fig. 6 (the non-extrapolated part of the plot) of [102], in terms of V_c (which is $2.8 \times 10^{-2} M_{\text{vir}}^{0.316}$ [111]).

We also found that the inner slope depends on the total baryonic content to total mass ratio [27], as seen later in [102].

[20, 21] show a comparison of the change of the inner slope with mass with the simulations of [102]. Moreover Figs. 4 and 5 in [20, 21], show a comparison of the Tully-Fisher, Faber-Jackson, $M_{\text{Star}} - M_{\text{halo}}$ relationships with simulations.

III. CLUSTERS

The cusp-core problem extends to the scales of cluster of galaxies: combining weak and strong lensing and stellar kinematics, the total inner density profile was shown as well described by dissipationless N-body simulations at radii $> 5 - 10$ kpc, while DM profiles are flatter than those obtained in the simulations [13, 14], within a radius of $\simeq 30$ kpc, typical of the Brightest Cluster Galaxy (BCG) radius. The DM profile is characterised by a variation of the slope, $\alpha = -d \log \rho_{\text{DM}}/d \log r$, from cluster to cluster which correlates with the BCG properties.

The total and the DM density profiles of MS2137, A963, A383, A611, A2537, A1667 and A2390, were determined in the aforementioned works. In [13, 14], improved data allowed

the determination of the stellar mass scale, allowing to produce a more physically consistent analysis, reducing the degeneracy among stellar and dark mass, and taking into account the BCGs homogeneity.

Two different approaches are available to compare the result of our model to the density profiles in [13]. While the density profile depends on the virial halo mass, M_{vir} , on the baryon fraction, $f_b = M_b/M_{\text{vir}}$, and on the random AM, as shown in [27], one can adjust the value of j , so that ρ_{DM} reproduces the observed clusters profiles. Here we rather prefer the possibility to “simulate” the formation and evolution of clusters with similar characteristics to those of [13]: final halo mass,³ M_{BCG} , core radius, etc.,⁴ by targeting not only the total halo and baryonic masses but also the observed radial density distribution (in the case of Fig. 1) and rotation curve (in the case of Fig. 3).

To obtain reasonable agreement between ours’ and observed clusters, we run simulations till the final halo and baryonic masses and corresponding radial density distributions differ by at most 10% from the observed clusters. To get this results the clusters were resimulated 50 times. To be precise, we iterated the model for each cluster 50 times until the produced clusters exhibited one with DM halo, gas, and stars masses and radial density profiles within 10% of the observed target.

Of all the seven cited clusters, in Fig. 1, we plot the spherically-averaged density profile of A2537 (studied by [12]), A611, and A2667 for the DM halo, BCG stars and their sum (total mass). The bottom blue band (upper green band) represents the DM (total mass) density profile determined by [13] for the clusters A611, A2537 (studied by [12]), and A2667, fitting the profile with a generalized Navarro-Frenk-White (gNFW) profile. The band in black dotted lines is the DM density profile obtained with the model of this paper. The band width represents the $1-\sigma$ uncertainty. The bottom arrow, in each panel, is the three-dimensional half-light radius of the BCG. The segment with slope $r^{-1.13}$ spans the radial range $r = [0.003 - 0.03]r_{200}$. The light blue line in the middle panel represents the NFW profile.

The plot shows a good agreement between the observations and the model: an inner DM profile with almost flat slopes in the case of A2537, and much more cuspy as in A611. However, in all the sample the inner slope has an average of $\simeq 0.54$, flatter than the NFW profile; a total mass profile close to a NFW profile and baryons dominate the profile in the inner $\simeq 10$ kpc.

In the left and right panels of Fig. 2, we show some correlations found by [14]. The points with error-bars in the middle panel show the value of the inner slope α vs the effective radius, R_e , of the BCG for the clusters indicated, obtained fitting their profiles with the generalized Navarro-Frenk-White

³ We use M_{200} as in [13]

⁴ By “simulate” we mean that, as in hydrodynamic simulations, we fix the initial conditions and follow the evolution of galaxies, or clusters, from the linear to the non-linear phase, until the object formation, and its subsequent evolution due to the physical effects previously described.

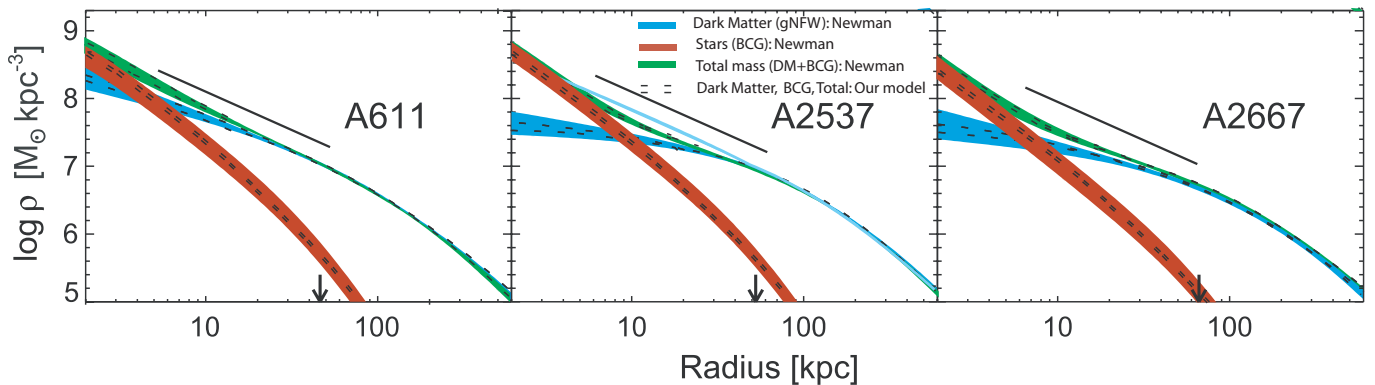


FIG. 1. Density profile of the total and DM mass for the clusters A611 (left panel), A2537 (middle panel) and A2667 (right panel). The bottom blue (upper green) band represents the DM (total mass) density profile determined by [13, 14], while the red band the stars' mass. The band in black dashed lines is the DM density profile obtained in this paper. The band widths represent the $1-\sigma$ uncertainty. The bottom arrow, in each panel, is the three-dimensional half-light radius of the BCG. The segment with slope $r^{-1.13}$ spans the radial range $r = [0.003 - 0.03]r_{200}$. The light blue line in the middle panel represents the NFW profile.

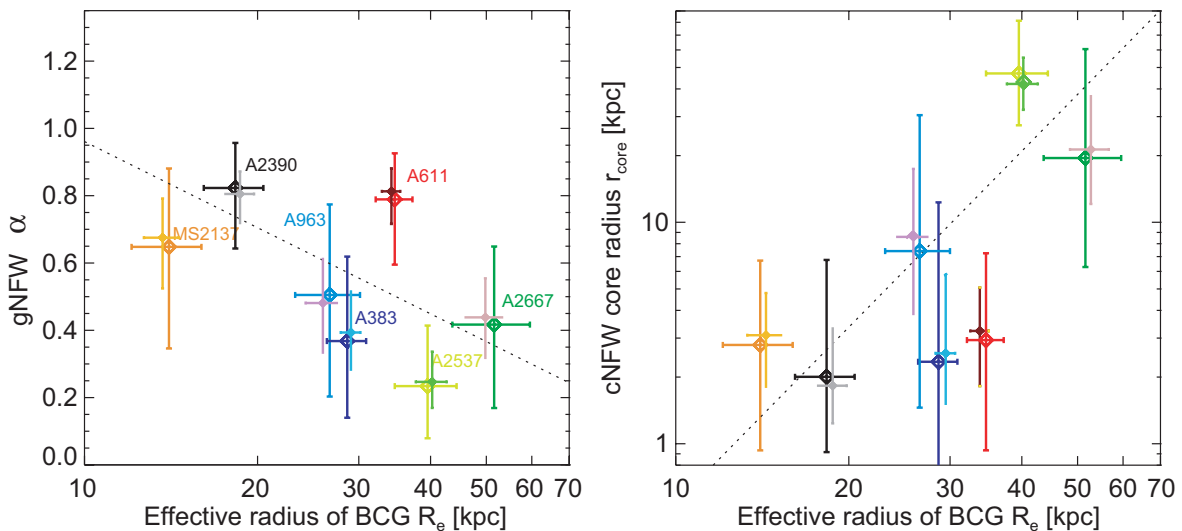


FIG. 2. Correlation among the inner DM profile and the BCG size. Left panel: inner slope of DM haloes, α vs the effective radius R_e of the BCG of the indicated clusters obtained fitting the clusters density profile with the gNFW model. The larger (smaller) error-bars correspond to the results by [14] (our model). The dotted lines are the least-square fits. Right panel: core radii, r_{core} , obtained fitting the clusters density profile with a cNFW model vs R_e .

profile (gNFW). The larger error bars represents the result by [14], the smaller ones, our results. The right panel represents the core radii, r_{core} , vs R_e for the same clusters, obtained fitting the density profiles with a cored NFW model (cNFW) [14]. Dotted lines are the least-square fits. We point out that while the correlations observed by [14] are re-obtained in our model, simulations, usually reaching mass scales of $10^{11} - 10^{12} M_{\odot}$, do not. Even the simulations by [56, 110] observe a flattening of the inner profile but do not study the correlations.

IV. DWARF AND LSBS GALAXIES

We use our model to simulate 100 galaxies in a Λ CDM cosmology with similar characteristics to the SPARC sample [112], a collection of nearby galaxies high-quality RCs. The stellar mass of the simulated sample is in the range $M_* = 6 \times 10^6 - 10^{11} M_{\odot}$. Of the galaxies used by [12], IC 2574, NGC 2366, DDO 154, UGC 4325, F563-V2, F563-1, F568-3, UGC 5750, F583-4, F583-1 are included in our larger sample.

The simulated objects produce a fair sample within the Λ CDM paradigm. The mass distribution follows the halo mass function. In particular we used [113]. The size distribution is a log-normal, as in ([114], Eq. (12)), and comes from the log-normal distribution of the spin parameter. The observed RCs were compared to the most similar simulated

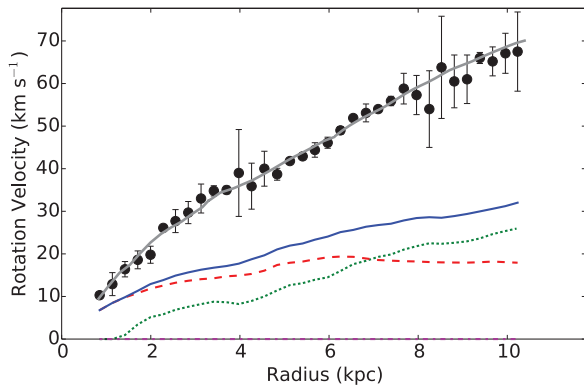


FIG. 3. Rotation curve of IC2574, dot with error bars, from the SPARC catalogue. The solid grey line is the RC of our model. The stars contribution to the RC is represented by the dotted green line, the gas disk by the dashed red line, and the total baryonic mass by the continuous blue line. This RC is presented for comparison with that shown by [12].

galaxies (e.g., with same halo and baryonic mass). Of particular interest, IC2574 can be mistaken as an outlier if the error bars, of $\simeq 5 - 10$ km/s, are not taken into account. However it lies in the outskirts of the distribution and we re-simulated it as we did previously for the clusters of our model to obtain an appropriately similar galaxy, within some percent, of the mass distributions of IC2574. Note that no further tuning was required. As an example, in Fig. 3, we show the RC of IC2574, the same reproduced by SIDM in [12].

Similarly to the case of clusters, we run several simulations for this galaxy until the final halo and baryonic masses⁵ differ by at most 10% from the observational data. The plot shows the observational RC (dots with error-bars), while the model prediction for the RC, the contribution to the RC given by gas, stars, and the total baryonic mass, are represented by the grey continuous line, red dashed line, green dotted line, and blue continuous line, respectively.

As can be seen here, the RC of IC2574 (advocated to be problematic for the scenario of core formation [16]) is very well described by the simulated galaxy, as well as the baryonic mass, as seen comparing with [115] or with the SPARC mass models [116]. We want to stress that the differences between the IC2574 RC’s baryon contribution (gas, stars) in [12] from that of SPARC or [115] arise from the different DM properties. The halo mass of the simulated galaxy host is $1.8 \times 10^{10} M_{\odot}$. We obtained the virial mass from the stellar mass using [117]. The stellar mass is $M_{*} = 10^{8.7} M_{\odot}$. The galaxy effective radius is $R_{\text{eff}} = 2.8$ kpc.

Recently [118] showed how the RC of IC2574 can be naturally obtained taking into account SN feedback, with a similar approach to ours.

⁵ Also, here, we refer not only to the total halo and baryonic masses but also the observed radial density distribution (RC).

V. DIVERSITY

Despite the fact that the RCs of dwarf galaxies are on average cored, individual fits to galaxy RCs show inner slopes ranging from $\alpha \simeq 0$ to cusps, while for cored profiles, the central densities can differ by a factor of 10 for galaxies inhabiting similar halos [120] and the situation becomes more complicated at higher masses. For many objects, [121] found cored and cuspy profiles in dwarfs which are similar while [122] observed a tendency to flatter profiles in less massive galaxies.

Such diversity was quantified by [16] comparing the circular velocity at 2 kpc, $V_{2\text{kpc}}$, with a fixed value of the maximum of circular velocity (V_{max}). For $50 < V_{\text{max}} < 250$ km/s there is a scatter of a few in $V_{2\text{kpc}}$. [15] studied the problem in the SIDM scenario, and found that SIDM alone cannot explain the scatter, since the resolution requires baryonic physics must also be taken into account.

In Fig. 3, we plot (left panel) $V_{2\text{kpc}}$ versus the outermost measured circular velocity V_{Rlast} . The dashed line is the expectation for a NFW density profile. The dots are the observed values from [112] and the open squares are the prediction of our model. The violet thick line represents the mean trend line. The sample obtained by [112] contains galaxies with stellar mass in the range $M_{*} \simeq 5 \times 10^6 - 10^{11.5} M_{\odot}$ corresponding to circular velocities in the range 15 – 300 km/s. In order to compare their results with our model, we chose simulated galaxies with stellar mass in the range of [112] and we calculated $V_{2\text{kpc}}$ and V_{Rlast} .⁶

As the dots show, at fixed V_{Rlast} , the scatter in $V_{2\text{kpc}}$ can be as large as a factor of four. Such scatter cannot be explained by the Λ CDM model, as it produces cuspy and self-similar halo density profiles, with a single parameter (concentration parameter or halo mass), in contrast to the cores displayed by many dwarfs. In the Λ CDM model, the much larger amount of DM in the halo cusp than the baryons “freezes” the scatter in $V_{2\text{kpc}}$, produced, conversely, by the spread in the baryon distribution. Baryon physics heats DM and enlarge the galaxies, reducing the inner DM content. As shown in [21, 22], the inner slope of the halo density profile is mass dependent. Milky Way-sized galaxies tend to have cuspy profiles while dwarf-sized galaxies cored profiles. Ultrafaint dwarf galaxies tend to be more cuspy than dwarfs. Therefore, the scatter seen in Fig. 3 originates from the mass dependence of the core formation process and the effects of environment, as described in [24].

Our model successfully recovers the scatter and distribution of the RCs shapes because baryon physics gives rise to different responses in the halo of simulated galaxies. The right panel of Fig. 4 represents the inner slope of the DM halo obtained in [102], dashed line, in the present paper, dot-dashed line, and in [119], solid line. All the curves were obtained as in [102] by fitting the DM profile with a power law in the radial range $0.01 < r/R_{\text{vir}} < 0.02$, being R_{vir} the virial radius.

⁶ Rlast for simulated galaxies is given from the linear fit to the SPARC galaxies distributed in the plane $M_{*} - \text{Rlast}$.

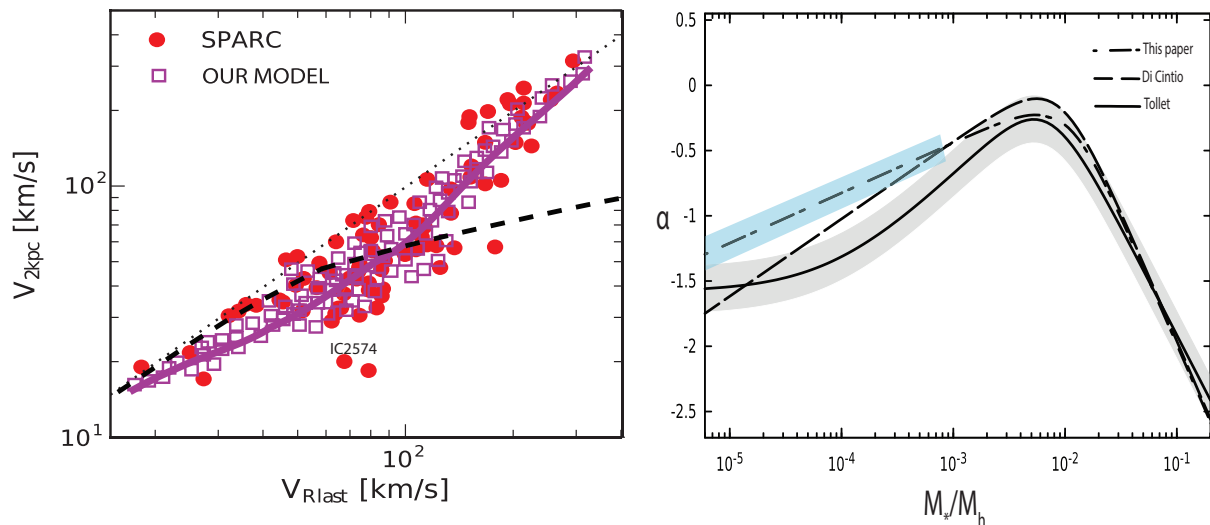


FIG. 4. Left panel: Effects of baryonic physics on the relation $V_{2\text{kpc}}-V_{\text{Rlast}}$. The dashed line represents the expectation if the haloes were all described by a NFW profile. The dots come from the SPARC galaxies of [112], while the open squares represent the prediction of our model. Right panel: Inner slope of the DM halo vs M_*/M_{halo} . The dashed line is the result of [102], the dot-dashed and the solid lines are the present paper and the results by [119]. The shaded blue and grey regions represent the $1-\sigma$ scatter in our result and [119], respectively.

The shaded blue and grey region represents the $1-\sigma$ scatter in our result and [119].

The plot shows that the core formation mechanism and α are strongly dependent on M_*/M_{halo} ⁷ with a minimum value of α at masses $M_*/M_{\text{halo}} \simeq 10^{-2}$ corresponding to $M_* \simeq 10^8 M_\odot$ [20, 102, 119] due to the maximum effects of baryon physics. For smaller masses the profile steepens because of the relative decrease of stars (ratio M_*/M_{halo}). Since the profile tends to steepen for $M_* \lesssim 10^8 M_\odot$ and V_{Rlast} is proportional to M_* , we should expect a self-similar behaviour, similar to the NFW RCs, as observed in Fig. 4, left panel. For $M_* \geq 10^8 M_\odot$, the increase in stellar masses gives rise to a deepening of the potential well and a reduction of the effects of baryon physics, with a consequent steepening of the profile. Notice that, because we account for star formation modification by AGN feedback which counters baryon cooling, our trend line agrees with SPARC at $V_{\text{Rlast}} \geq 150$ km/s. Moreover, hydrodynamics simulations usually examine isolated galaxies while in our model the account of tidal interactions makes it more environment dependent.

VI. CONCLUSIONS

The Λ CDM model exhibits some problems at small scales, and in particular predicts an excess of DM in the central parts of galaxies and clusters. In this paper, we showed that a unified solution to the problem can be obtained within the Λ CDM framework without introducing different forms of DM [as done in 12, instead]. With a semi-analytic model whose main mechanism is based on dynamical friction, we simulated

the clusters studied by [14] and compared the density profiles with those they obtained: those profiles were re-obtained correctly by our model.

We displayed one of those density profiles (Fig. 1).

We then simulated a sample of galaxies similar to the SPARC compilation, also containing the galaxies studied by [12], finding again a good agreement with data, as shown in the case of one of the most complicated galaxy RCs to reproduce, namely that of IC2574 (Fig. 3).

We want to stress that to match observations we re-simulated the object studied by targeting not only the total halo and baryonic masses but also the observed radial density distribution (in the case of Fig. 1) and rotation curve (in the case of Fig. 3).

Finally, we studied the “diversity” problem using the simulated galaxies, and comparing their $V_{2\text{kpc}}$, for given values of V_{Rlast} with the compilation in [112]. We show that baryon physics gives rise to RCs very different from each other, due to the dependence of the RC from their total and stellar mass, together with environment. This explains the scatter in the $V_{2\text{kpc}}-V_{\text{Rlast}}$ plane.

ACKNOWLEDGEMENTS

F.P. acknowledges support from STFC grant ST/P000649/1. A.D.P. was supported by the Chinese Academy of Sciences and by the Presidents International Fellowship Initiative, Grant No. 2017 VMA0044. The authors thank an anonymous referee whose comments helped to improve the scientific content of this work.

⁷ The correlation between α and M_*/M_{halo} can be expressed in terms of

M_* , using for example the relation in [117].

- [1] D. N. Spergel, L. Verde, H. V. Peiris, E. Komatsu, M. R.olta, C. L. Bennett, M. Halpern, G. Hinshaw, N. Jarosik, A. Kogut, M. Limon, S. S. Meyer, L. Page, G. S. Tucker, J. L. Weiland, E. Wollack, and E. L. Wright, *ApJS* **148**, 175 (2003), [astro-ph/0302209](#).
- [2] E. Komatsu, K. M. Smith, J. Dunkley, and et al., *ApJS* **192**, 18 (2011), [arXiv:1001.4538 \[astro-ph.CO\]](#).
- [3] S. Weinberg, *Reviews of Modern Physics* **61**, 1 (1989).
- [4] A. V. Astashenok and A. del Popolo, *Classical and Quantum Gravity* **29**, 085014 (2012), [arXiv:1203.2290 \[gr-qc\]](#).
- [5] J. F. Navarro, C. S. Frenk, and S. D. M. White, *ApJ* **462**, 563 (1996), [astro-ph/9508025](#).
- [6] B. Moore, *Nature (London)* **370**, 629 (1994).
- [7] R. A. Flores and J. R. Primack, *ApJL* **427**, L1 (1994), [astro-ph/9402004](#).
- [8] V. F. Cardone and A. Del Popolo, *MNRAS* **427**, 3176 (2012), [arXiv:1209.1524 \[astro-ph.CO\]](#).
- [9] M. Boylan-Kolchin, J. S. Bullock, and M. Kaplinghat, *MNRAS* **415**, L40 (2011), [arXiv:1103.0007 \[astro-ph.CO\]](#).
- [10] E. Papastergis, R. Giovanelli, M. P. Haynes, and F. Shankar, *A&A* **574**, A113 (2015), [arXiv:1407.4665](#).
- [11] D. N. Spergel and P. J. Steinhardt, *Physical Review Letters* **84**, 3760 (2000), [astro-ph/9909386](#).
- [12] M. Kaplinghat, S. Tulin, and H.-B. Yu, *Physical Review Letters* **116**, 041302 (2016), [arXiv:1508.03339](#).
- [13] A. B. Newman, T. Treu, R. S. Ellis, D. J. Sand, C. Nipoti, J. Richard, and E. Jullo, *ApJ* **765**, 24 (2013), [arXiv:1209.1391 \[astro-ph.CO\]](#).
- [14] A. B. Newman, T. Treu, R. S. Ellis, and D. J. Sand, *ApJ* **765**, 25 (2013), [arXiv:1209.1392 \[astro-ph.CO\]](#).
- [15] P. Creasey, O. Sameie, L. V. Sales, H.-B. Yu, M. Vogelsberger, and J. Zavala, *MNRAS* **468**, 2283 (2017), [arXiv:1612.03903](#).
- [16] K. A. Oman, J. F. Navarro, A. Fattahi, C. S. Frenk, T. Sawala, S. D. M. White, R. Bower, R. A. Crain, M. Furlong, M. Schaller, J. Schaye, and T. Theuns, *MNRAS* **452**, 3650 (2015), [arXiv:1504.01437](#).
- [17] A. Del Popolo, *ApJ* **698**, 2093 (2009), [arXiv:0906.4447 \[astro-ph.CO\]](#).
- [18] A. Del Popolo and P. Kroupa, *A&A* **502**, 733 (2009), [arXiv:0906.1146 \[astro-ph.CO\]](#).
- [19] A. Del Popolo and N. Hieltel, *JCAP* **1**, 047 (2014), [arXiv:1401.6577 \[astro-ph.GA\]](#).
- [20] A. Del Popolo and F. Pace, *Astrophysics and Space Science* **361**, 162 (2016), [arXiv:1502.01947](#).
- [21] A. Del Popolo, *Astrophysics and Space Science* **361**, 222 (2016), [arXiv:1607.07408](#).
- [22] A. Del Popolo, *MNRAS* **408**, 1808 (2010), [arXiv:1012.4322 \[astro-ph.CO\]](#).
- [23] A. Del Popolo, *JCAP* **7**, 014 (2011), [arXiv:1112.4185 \[astro-ph.CO\]](#).
- [24] A. Del Popolo, *MNRAS* **419**, 971 (2012), [arXiv:1105.0090 \[astro-ph.CO\]](#).
- [25] A. Del Popolo, *International Journal of Modern Physics D* **23**, 1430005 (2014), [arXiv:1305.0456 \[astro-ph.CO\]](#).
- [26] A. Del Popolo, in *AIP Conf. Proc.*, Vol. 1548 (2013) pp. 2–63.
- [27] A. Del Popolo, *MNRAS* **424**, 38 (2012), [arXiv:1204.4439 \[astro-ph.CO\]](#).
- [28] A. Del Popolo, V. F. Cardone, and G. Belvedere, *MNRAS* **429**, 1080 (2013), [arXiv:1212.6797 \[astro-ph.CO\]](#).
- [29] J. E. Gunn and J. R. Gott, III, *ApJ* **176**, 1 (1972).
- [30] E. Bertschinger, *ApJS* **58**, 39 (1985).
- [31] Y. Hoffman and J. Shaham, *ApJ* **297**, 16 (1985).
- [32] B. S. Ryden and J. E. Gunn, *ApJ* **318**, 15 (1987).
- [33] Y. Ascasibar, G. Yepes, S. Gottlöber, and V. Müller, *MNRAS* **352**, 1109 (2004), [arXiv:astro-ph/0312221](#).
- [34] L. L. R. Williams, A. Babul, and J. J. Dalcanton, *ApJ* **604**, 18 (2004), [arXiv:astro-ph/0312002](#).
- [35] B. S. Ryden, *ApJ* **329**, 589 (1988).
- [36] A. Del Popolo and M. Gambera, *A&A* **321**, 691 (1997), [astro-ph/9610052](#).
- [37] A. Del Popolo and M. Gambera, *A&A* **357**, 809 (2000), [astro-ph/9909156](#).
- [38] A. Del Popolo, F. Pace, and J. A. S. Lima, *International Journal of Modern Physics D* **22**, 1350038 (2013), [arXiv:1207.5789 \[astro-ph.CO\]](#).
- [39] A. Del Popolo, F. Pace, and J. A. S. Lima, *MNRAS* **430**, 628 (2013), [arXiv:1212.5092 \[astro-ph.CO\]](#).
- [40] A. Del Popolo, F. Pace, S. P. Maydanyuk, J. A. S. Lima, and J. F. Jesus, *Phys. Rev. D* **87**, 043527 (2013), [arXiv:1303.3628 \[astro-ph.CO\]](#).
- [41] F. Pace, R. C. Batista, and A. Del Popolo, *MNRAS* **445**, 648 (2014), [arXiv:1406.1448](#).
- [42] A. El-Zant, I. Shlosman, and Y. Hoffman, *ApJ* **560**, 636 (2001), [astro-ph/0103386](#).
- [43] A. A. El-Zant, Y. Hoffman, J. Primack, F. Combes, and I. Shlosman, *ApJL* **607**, L75 (2004), [astro-ph/0309412](#).
- [44] C.-P. Ma and M. Boylan-Kolchin, *Physical Review Letters* **93**, 021301 (2004), [astro-ph/0403102](#).
- [45] E. Romano-Díaz, I. Shlosman, Y. Hoffman, and C. Heller, *ApJL* **685**, L105 (2008), [arXiv:0808.0195](#).
- [46] E. Romano-Díaz, I. Shlosman, C. Heller, and Y. Hoffman, *ApJ* **702**, 1250 (2009), [arXiv:0901.1317 \[astro-ph.CO\]](#).
- [47] D. R. Cole, W. Dehnen, and M. I. Wilkinson, *MNRAS* **416**, 1118 (2011), [arXiv:1105.4050 \[astro-ph.CO\]](#).
- [48] S. Inoue and T. R. Saitoh, *MNRAS* **418**, 2527 (2011), [arXiv:1108.0906 \[astro-ph.CO\]](#).
- [49] C. Nipoti and J. Binney, *MNRAS* **446**, 1820 (2015), [arXiv:1410.6169](#).
- [50] G. R. Blumenthal, S. M. Faber, R. Flores, and J. R. Primack, *ApJ* **301**, 27 (1986).
- [51] O. Y. Gnedin, A. V. Kravtsov, A. A. Klypin, and D. Nagai, *ApJ* **616**, 16 (2004), [astro-ph/0406247](#).
- [52] A. Klypin, H. Zhao, and R. S. Somerville, *ApJ* **573**, 597 (2002), [astro-ph/0110390](#).
- [53] M. Gustafsson, M. Fairbairn, and J. Sommer-Larsen, *Phys. Rev. D* **74**, 123522 (2006), [astro-ph/0608634](#).
- [54] G. De Lucia and A. Helmi, *MNRAS* **391**, 14 (2008), [arXiv:0804.2465](#).
- [55] Y.-S. Li, G. De Lucia, and A. Helmi, *MNRAS* **401**, 2036 (2010), [arXiv:0909.1291 \[astro-ph.GA\]](#).
- [56] D. Martizzi, R. Teyssier, B. Moore, and T. Wentz, *MNRAS* **422**, 3081 (2012), [arXiv:1112.2752 \[astro-ph.CO\]](#).
- [57] J. I. Read and G. Gilmore, *MNRAS* **356**, 107 (2005), [astro-ph/0409565](#).
- [58] A. Pontzen and F. Governato, *MNRAS* **421**, 3464 (2012), [arXiv:1106.0499 \[astro-ph.CO\]](#).
- [59] R. Teyssier, A. Pontzen, Y. Dubois, and J. I. Read, *MNRAS* **429**, 3068 (2013), [arXiv:1206.4895 \[astro-ph.CO\]](#).
- [60] J. E. Gunn, *ApJ* **218**, 592 (1977).
- [61] J. A. Fillmore and P. Goldreich, *ApJ* **281**, 1 (1984).
- [62] E. Komatsu, J. Dunkley, M. R.olta, and et al., *ApJS* **180**, 330 (2009), [arXiv:0803.0547](#).

- [63] F. Hoyle, *ApJ* **118**, 513 (1953).
- [64] P. J. E. Peebles, *ApJ* **155**, 393 (1969).
- [65] S. D. M. White, *ApJ* **286**, 38 (1984).
- [66] D. J. Eisenstein and A. Loeb, *ApJ* **439**, 520 (1995), [arXiv:astro-ph/9405012](#).
- [67] N. Hiodelis and A. del Popolo, *MNRAS* **436**, 163 (2013).
- [68] V. Avila-Reese, C. Firmani, and X. Hernández, *ApJ* **505**, 37 (1998), [astro-ph/9710201](#).
- [69] E. Spedicato, E. Bodon, A. D. Popolo, and N. Mahdavi-Amiri, *Quarterly Journal of the Belgian, French and Italian Operations Research Societies* **1**, 51 (2003).
- [70] A. Toomre, *ApJ* **139**, 1217 (1964).
- [71] J. Binney and S. Tremaine, *Princeton, NJ, Princeton University Press, 1987*, 747 p. (1987).
- [72] M. R. Krumholz and A. Dekel, *MNRAS* **406**, 112 (2010), [arXiv:1001.0765](#).
- [73] A. Dekel, R. Sari, and D. Ceverino, *ApJ* **703**, 785 (2009), [arXiv:0901.2458 \[astro-ph.GA\]](#).
- [74] D. Ceverino, A. Dekel, N. Mandelker, F. Bournaud, A. Burkert, R. Genzel, and J. Primack, *MNRAS* **420**, 3490 (2012), [arXiv:1106.5587](#).
- [75] C. Nipoti, T. Treu, L. Ciotti, and M. Stiavelli, *MNRAS* **355**, 1119 (2004), [astro-ph/0404127](#).
- [76] A. Del Popolo and M. Le Delliou, *JCAP* **12**, 051 (2014), [arXiv:1408.4893](#).
- [77] D. Ceverino, A. Dekel, and F. Bournaud, *MNRAS* **404**, 2151 (2010), [arXiv:0907.3271 \[astro-ph.CO\]](#).
- [78] J. Perez, O. Valenzuela, P. B. Tissera, and L. Michel-Dansac, *MNRAS* **436**, 259 (2013), [arXiv:1308.4396](#).
- [79] F. Bournaud, V. Perret, F. Renaud, A. Dekel, B. G. Elmegreen, D. M. Elmegreen, R. Teyssier, P. Amram, E. Daddi, P.-A. Duc, D. Elbaz, B. Epinat, J. M. Gabor, S. Juneau, K. Kraljic, and E. Le Floch, *ApJ* **780**, 57 (2014), [arXiv:1307.7136 \[astro-ph.CO\]](#).
- [80] D. Ceverino, A. Klypin, E. S. Klimek, S. Trujillo-Gomez, C. W. Churchill, J. Primack, and A. Dekel, *MNRAS* **442**, 1545 (2014), [arXiv:1307.0943](#).
- [81] V. Perret, F. Renaud, B. Epinat, P. Amram, F. Bournaud, T. Contini, R. Teyssier, and J.-C. Lambert, *A&A* **562**, A1 (2014), [arXiv:1307.7130](#).
- [82] D. Ceverino, A. Dekel, D. Tweed, and J. Primack, *MNRAS* **447**, 3291 (2015), [arXiv:1409.2622](#).
- [83] M. Behrendt, A. Burkert, and M. Schartmann, *ApJL* **819**, L2 (2016), [arXiv:1512.03430](#).
- [84] D. M. Elmegreen, B. G. Elmegreen, and A. C. Hirst, *ApJL* **604**, L21 (2004), [astro-ph/0402477](#).
- [85] D. M. Elmegreen, B. G. Elmegreen, M. T. Marcus, K. Shahinyan, A. Yau, and M. Petersen, *ApJ* **701**, 306 (2009), [arXiv:0906.2660 \[astro-ph.CO\]](#).
- [86] R. Genzel, S. Newman, T. Jones, N. M. Förster Schreiber, K. Shapiro, S. Genel, S. J. Lilly, and et al., *ApJ* **733**, 101 (2011), [arXiv:1011.5360 \[astro-ph.CO\]](#).
- [87] Y. Guo, M. Giavalisco, H. C. Ferguson, P. Cassata, and A. M. Koekemoer, *ApJ* **757**, 120 (2012), [arXiv:1110.3800](#).
- [88] S. Wuyts, N. M. Förster Schreiber, E. J. Nelson, P. G. van Dokkum, G. Brammer, Y.-Y. Chang, S. M. Faber, H. C. Ferguson, M. Franx, M. Fumagalli, R. Genzel, N. A. Grogin, D. D. Kocevski, A. M. Koekemoer, B. Lundgren, D. Lutz, E. J. McGrath, I. Momcheva, D. Rosario, R. E. Skelton, L. J. Tacconi, A. van der Wel, and K. E. Whitaker, *ApJ* **779**, 135 (2013), [arXiv:1310.5702](#).
- [89] Y. Guo, H. C. Ferguson, E. F. Bell, D. C. Koo, C. J. Conselice, M. Giavalisco, S. Kassin, Y. Lu, R. Lucas, N. Mandelker, D. M. McIntosh, J. R. Primack, S. Ravindranath, G. Barro, D. Ceverino, A. Dekel, S. M. Faber, J. J. Fang, A. M. Koekemoer, K. Noeske, M. Rafelski, and A. Straughn, *ApJ* **800**, 39 (2015), [arXiv:1410.7398](#).
- [90] D. M. Elmegreen, B. G. Elmegreen, S. Ravindranath, and D. A. Coe, *ApJ* **658**, 763 (2007), [astro-ph/0701121](#).
- [91] M. Noguchi, *Nature (London)* **392**, 253 (1998).
- [92] M. Noguchi, *ApJ* **514**, 77 (1999), [astro-ph/9806355](#).
- [93] M. Aumer, A. Burkert, P. H. Johansson, and R. Genzel, *ApJ* **719**, 1230 (2010), [arXiv:1007.0169](#).
- [94] H. Baumgardt and P. Kroupa, *MNRAS* **380**, 1589 (2007), [arXiv:0707.1944](#).
- [95] M. R. Krumholz and J. C. Tan, *ApJ* **654**, 304 (2007), [astro-ph/0606277](#).
- [96] B. G. Elmegreen, F. Bournaud, and D. M. Elmegreen, *ApJ* **688**, 67 (2008), [arXiv:0808.0716](#).
- [97] B. G. Elmegreen, D. M. Elmegreen, J. Sánchez Almeida, C. Muñoz-Tuñón, J. Dewberry, J. Putko, Y. Teich, and M. Popinchalk, *ApJ* **774**, 86 (2013), [arXiv:1308.0306](#).
- [98] C. A. Garland, D. J. Pisano, M.-M. Mac Low, K. Kreckel, K. Rabidoux, and R. Guzmán, *ApJ* **807**, 134 (2015), [arXiv:1506.04649](#).
- [99] N. Mandelker, A. Dekel, D. Ceverino, C. DeGraf, Y. Guo, and J. Primack, *MNRAS* **464**, 635 (2017), [arXiv:1512.08791](#).
- [100] A. V. Kravtsov, O. Y. Gnedin, and A. A. Klypin, *ApJ* **609**, 482 (2004), [astro-ph/0401088](#).
- [101] S. D. M. White and C. S. Frenk, *ApJ* **379**, 52 (1991).
- [102] A. Di Cintio, C. B. Brook, A. V. Macciò, G. S. Stinson, A. Knebe, A. A. Dutton, and J. Wadsley, *MNRAS* **437**, 415 (2014), [arXiv:1306.0898 \[astro-ph.CO\]](#).
- [103] D. J. Croton, V. Springel, S. D. M. White, G. De Lucia, C. S. Frenk, L. Gao, A. Jenkins, G. Kauffmann, J. F. Navarro, and N. Yoshida, *MNRAS* **365**, 11 (2006), [astro-ph/0508046](#).
- [104] G. Chabrier, *PASP* **115**, 763 (2003), [astro-ph/0304382](#).
- [105] A. Cattaneo, A. Dekel, J. Devriendt, B. Guiderdoni, and J. Blaizot, *MNRAS* **370**, 1651 (2006), [astro-ph/0601295](#).
- [106] D. Martizzi, R. Teyssier, and B. Moore, *MNRAS* **420**, 2859 (2012), [arXiv:1106.5371 \[astro-ph.CO\]](#).
- [107] C. M. Booth and J. Schaye, *MNRAS* **398**, 53 (2009), [arXiv:0904.2572](#).
- [108] F. Governato, C. Brook, L. Mayer, A. Brooks, G. Rhee, J. Wadsley, P. Jonsson, B. Willman, G. Stinson, T. Quinn, and P. Madau, *Nature (London)* **463**, 203 (2010), [arXiv:0911.2237 \[astro-ph.CO\]](#).
- [109] F. Governato, A. Zolotov, A. Pontzen, C. Christensen, S. H. Oh, A. M. Brooks, T. Quinn, S. Shen, and J. Wadsley, *MNRAS* **422**, 1231 (2012), [arXiv:1202.0554 \[astro-ph.CO\]](#).
- [110] D. Martizzi, R. Teyssier, and B. Moore, *MNRAS* **432**, 1947 (2013), [arXiv:1211.2648](#).
- [111] A. A. Klypin, S. Trujillo-Gomez, and J. Primack, *ApJ* **740**, 102 (2011), [arXiv:1002.3660](#).
- [112] F. Lelli, S. S. McGaugh, and J. M. Schombert, *AJ* **152**, 157 (2016), [arXiv:1606.09251](#).
- [113] A. Del Popolo, F. Pace, and M. Le Delliou, *JCAP* **3**, 032 (2017), [arXiv:1703.06918](#).
- [114] S. Shen, H. J. Mo, S. D. M. White, M. R. Blanton, G. Kauffmann, W. Voges, J. Brinkmann, and I. Csabai, *MNRAS* **343**, 978 (2003), [astro-ph/0301527](#).
- [115] S. Blais-Ouellette, P. Amram, and C. Carignan, *AJ* **121**, 1952 (2001), [astro-ph/0006449](#).
- [116] S.-H. Oh, W. J. G. de Blok, F. Walter, E. Brinks, and R. C. Kennicutt, Jr., *AJ* **136**, 2761 (2008), [arXiv:0810.2119](#).
- [117] B. P. Moster, T. Naab, and S. D. M. White, *MNRAS* **428**, 3121 (2013), [arXiv:1205.5807 \[astro-ph.CO\]](#).

- [118] I. M. Santos-Santos, A. Di Cintio, C. B. Brook, A. Macciò, A. Dutton, and R. Domínguez-Tenreiro, ArXiv e-prints (2017), [arXiv:1706.04202](#).
- [119] E. Tollet, A. V. Macciò, A. A. Dutton, G. S. Stinson, L. Wang, C. Penzo, T. A. Gutcke, T. Buck, X. Kang, C. Brook, A. Di Cintio, B. W. Keller, and J. Wadsley, *MNRAS* **456**, 3542 (2016), [arXiv:1507.03590](#).
- [120] R. Kuzio de Naray, G. D. Martinez, J. S. Bullock, and M. Kaplinghat, *ApJL* **710**, L161 (2010), [arXiv:0912.3518](#).
- [121] J. D. Simon, A. D. Bolatto, A. Leroy, L. Blitz, and E. L. Gates, *ApJ* **621**, 757 (2005), [astro-ph/0412035](#).
- [122] W. J. G. de Blok, F. Walter, E. Brinks, C. Trachternach, S.-H. Oh, and R. C. Kennicutt, Jr., *AJ* **136**, 2648 (2008), [arXiv:0810.2100](#).